

Manuscript Number:

Title: Sedimentology and composition of sands injected during the seismic crisis of May 2012 (Emilia, Italy): clues for source layer identification and liquefaction regime

Article Type: Research Paper

Keywords: Sand liquefaction, sand composition, 2012 Emilia Romagna earthquake, fluvial deposits, Po Plain.

Corresponding Author: Prof. Stefano Lugli,

Corresponding Author's Institution: Università degli Studi di Modena e Reggio Emilia

First Author: Daniela Fontana

Order of Authors: Daniela Fontana; Stefano Lugli; Simona Marchetti Dori; Riccardo Caputo; Marco Stefani

Abstract: In May 2012 widespread sand blows formed along buried channels in the eastern sector of the Po Plain as a consequence of a seismic crisis with main shocks of Mw 6.1 and 5.9. At San Carlo (Ferrara) a trench dug a few week after the earthquakes exposed sand dikes cutting through an old Reno River channel-levee system that was diverted in the 18^o century and was deposited starting from the 14^o century (unit A); this sequence lie on Holocene muddy floodplain and scattered sandy channel deposits (unit B) and a Pleistocene channel sand unit (unit C). Sand inverse and direct grading, concave layering and vertical lamination coexisting along the dikes suggest multiple rhythmic opening and closing of the fracture borders that were injected and filled of slurry sand during the compression pulses end emptied during the extension phase. The pulse mechanism may have lasted for several minutes and formed well stratified structure of the sand volcanoes that formed on the top of some fractures. Sands from dikes and from the various units show well defined compositional fields from lithoarenitic to quartz-feldspar-rich compositions. Sorting related to sediment flux variations did not apparently affect the sand composition, across the sedimentary structures. Sands from the old Reno levee and channel fill (unit A) have abundant lithic fragments deriving from the erosion of Apennine sedimentary carbonate and terrigenous successions. Pleistocene sands (unit C) are enriched in quartz and feldspars as a consequence of the different climatic weathering condition that prevailed during the last glacial stage. The Pleistocene sand were partially reworked during the Holocene (unit B). Composition of the sand filling the dikes show clear affinities with sand layer of the old Reno River channel (Unit A) and clearly differ from any sand from deeper layers (Unit B and C), which are richer in quartz and feldspar and poorer in sedimentary lithic fragments. Textural and compositional data indicate that the liquefaction processes originated from a relatively shallow source consisting of channel sands located within Unit A at 6.8.to 7.5 m depth.

Suggested Reviewers: José Arribas Mocoora
Universidad Complutense Madrid
arribas@geo.ucm.es
expert

Gert Jan Weltje

Delft University of Technology
G.J.Weltje@tudelft.nl

Franco Ricci Lucchi
Università di Bologna, retired
riccilucchi@msn.com

AKM Khorshed Alam
Geological Survey of Bangladesh
akmkhorshed@gmail.com

Abhijit Basu
Indiana University
basu@indiana.edu

Cristina Stefani
Università di Padova
cristina.stefani@unipd.it

Mark Johnsson
California Coastal Commission
mark.johnsson@coastal.ca.gov

Dear Editors,

We are submitting the manuscript "Sedimentology and composition of sands injected during the seismic crisis of May 2012 (Emilia, Italy): clues for source layer identification and liquefaction regime", that we would like you to be considered for publication on Sedimentary Geology.

The manuscript deals with the detailed facies texture and petrographic composition of sands ejected during the 2012 Emilia earthquake (Italy) in order to identify the source layer and to provide a contribution to the understanding of earthquake-induced liquefaction mechanisms.

We think that our work could be of interest for the Sedimentary Geology readers.

Best regards,

D. Fontana, S. Lugli, S. Marchetti Dori, R. Caputo and M. Stefani

Highlights

Composition of injected sand of 2012 Emilia earthquake help pinpoint source layer

Fluvial sands at different stratigraphic have distinct petrographic composition

Sedimentology of dike sand suggest multiple rhythmic fracture opening-closing

Sorting due to flux variation did not affect sand composition

1 **Sedimentology and composition of sands injected during the seismic crisis of May 2012**
2 **(Emilia, Italy): clues for source layer identification and liquefaction regime**

3
4 D. Fontana^a, S. Lugli^a, S. Marchetti Dori^a, R. Caputo^b and M. Stefani^b

5
6 ^a Dipartimento di Scienze Chimiche e Geologiche, Università di Modena e Reggio Emilia, via
7 S. Eufemia 19, 41125 Modena; corresponding author: stefano.lugli@unimore.it

8 ^b Dipartimento di Fisica e Scienze della Terra, Università di Ferrara, Via Saragat 1, 44122
9 Ferrara.

10

11

12 **ABSTRACT**

13 In May 2012 widespread sand blows formed along buried channels in the eastern sector of the Po
14 Plain as a consequence of a seismic crisis with main shocks of Mw 6.1 and 5.9. At San Carlo
15 (Ferrara) a trench dug a few week after the earthquakes exposed sand dikes cutting through an old
16 Reno River channel-levee system that was diverted in the 18^o century and was deposited starting
17 from the 14^o century (unit A); this sequence lie on Holocene muddy floodplain and scattered sandy
18 channel deposits (unit B) and a Pleistocene channel sand unit (unit C). Sand inverse and direct
19 grading, concave layering and vertical lamination coexisting along the dikes suggest multiple
20 rhythmic opening and closing of the fracture borders that were injected and filled of slurry sand
21 during the compression pulses end emptied during the extension phase. The pulse mechanism may
22 have lasted for several minutes and formed well stratified structure of the sand volcanoes that
23 formed on the top of some fractures. Sands from dikes and from the various units show well defined
24 compositional fields from lithoarenitic to quartz-feldspar-rich compositions. Sorting related to
25 sediment flux variations did not apparently affect the sand composition, across the sedimentary
26 structures. Sands from the old Reno levee and channel fill (unit A) have abundant lithic fragments

27 deriving from the erosion of Apennine sedimentary carbonate and terrigenous successions.
28 Pleistocenic sands (unit C) are enriched in quartz and feldspars as a consequence of the different
29 climatic weathering condition that prevailed during the last glacial stage. The Pleistocene sands
30 were partially reworked during the Holocene (unit B). Composition of the sand filling the dikes
31 show clear affinities with sand layer of the old Reno River channel (Unit A) and clearly differ from
32 any sand from deeper layers (Unit B and C), which are richer in quartz and feldspar and poorer in
33 sedimentary lithic fragments. Textural and compositional data indicate that the liquefaction
34 processes originated from a relatively shallow source consisting of channel sands located within
35 Unit A at 6.8.to 7.5 m depth.

36

37 *Keywords:* Sand liquefaction, sand composition, 2012 Emilia Romagna earthquake, fluvial
38 deposits, Po Plain.

39

40 **1. Introduction**

41

42 In May 2012 the eastern sector of the Po Plain (northern Italy) was affected by two
43 earthquakes (Mw 6.1 and 5.9; Pondrelli et al., 2012) followed by several aftershocks (up to
44 Mw 5.1). The seismic crisis was triggered in correspondence of a portion of the Apennines
45 thrust belt buried below the alluvial plain (Pieri and Groppi, 1981; Caputo et al., 2012). The
46 first event produced relevant liquefaction phenomena, surface fracturing and sand ejection, in
47 particular in the western sector of the Ferrara province (Papathanassiou et al., 2012). In this
48 area, the liquefaction processes were concentrated along an elongated topographic ridge
49 corresponding to an old channel of the Reno River that was active until the end of the 18^o
50 century when it was artificially diverted.

51 Due to the destructive damage potentially produced on human structures and activities, sand
52 boil and liquefaction phenomena are throughly studied to asses the geotechnical conditions for

53 their recurrence (Chang et al., 2011). Less explored is the sedimentology of the liquefaction
54 mechanisms and the selective processes acting on sand grains: This is particularly interesting
55 because, although the phenomenon is mostly limited to sands, even gravelly sediments can be
56 susceptible to liquefaction (Chen et al., 2008). No data are available on the possible influence
57 of the liquefaction phenomena on the sediment composition: does sand retain the same
58 petrographic composition of the source layer while travelling through the fractures? Is there
59 any selective mechanism that may shift the sediment composition when the pressurized slurry
60 of water and sand erupts to the ground surface? These questions are particularly significant as
61 the sand composition may be used as a tool to pinpoint the source layers, provided that sands
62 located at different stratigraphic layers have been petrographically characterized. This applies
63 also to old sand blows buried by other deposits preserved in the geologic record.

64 Fluvial sand composition studies have a particular significance in depositional settings such as
65 the late Pleistocene–Holocene Po Plain, where distinct compositional fields characterize
66 modern sands from different streams, as well as older sediments, back to the Pleistocene
67 (Lugli et al., 2007; Garzanti et al., 2011). Several key petrographic components provide
68 diagnostic features to distinguish sand bodies buried beneath the floodplain (Johnsson et al,
69 1991; Arribas and Tortosa, 2003; Critelli et al., 2003; Weltje and Von Eynatten, 2004; Basu et
70 al., 2013). In this context, we analyzed the texture and petrographic composition of sands
71 injected during the seismic crisis of 2012 along the paleo-Reno River body at San Carlo
72 (Ferrara), and sands from subsurface deposits at different depths. The aim of the research was
73 to provide a contribution to the understanding of earthquake-induced liquefaction mechanisms
74 using texture and petrographic parameters to identify the possible source layers of the sand
75 blows.

76

77 **2. Geological setting**

78

79 The Ferrara alluvial plain area is located on the northern buried sector of the northern
80 Apennines fold-and-thrust belt, where streams draining the chain flow northeastward into the
81 Po River and the Adriatic Sea (Fig. 1). The Northern Apennines formed mainly during the
82 Tertiary in the frame of the convergence between the European and the Adria plates. The plate
83 movement consumed the interposed Tethyan oceanic crust with the formation of an
84 accretionary prism, which during the subsequent collisional phase produced a complex
85 orogenic wedge (Ricci Lucchi, 1986; Bettelli and De Nardo, 2001; Argnani et al., 2004). On
86 the northern side of the chain, these units are unconformably overlain by Miocene-Pliocene
87 and Quaternary terrigenous deposits of the Po Plain.

88 The Po Plain is the syntectonic sedimentary wedge filling the Pliocene-Pleistocene Apennine
89 foredeep. The total basin infill is up to 4 km-thick, and the Quaternary deposits reach a
90 thickness of 1.5 km. The factors controlling the architecture of the sedimentary filling
91 (Amorosi et al., 2008) were the contrasting subsidence average rates induced by the vertical
92 motions of the blind thrusts buried under the foredeep deposits, such as the Ferrara fault-fold
93 system (Pieri and Groppi, 1981). This long-term effect combined with the Holocene rise of
94 the Adriatic Sea level reduced the gradient along a west-east drainage axis. The main drainage
95 element, the Po River, was tectonically forced to shift northwards and human pressure on
96 forest cover since the Bronze Age produced a generalized increase in fine bedload discharge
97 into the Apennines tributaries (Ravazzi et al., 2013). The river network continuously shifted
98 laterally as a consequence of climate changes and to adjust the local tectonic pattern (Fig.1).

99 The late evolution of the system has been successfully traced following the physical evidence
100 of paleochannels on the alluvial plain surface, whereas the older sedimentary patterns are
101 revealed by the provenance composition signal of buried Holocene channel sands which match
102 those of the present day rivers (Lugli et al., 2007).

103

104 **3. The recent evolution of the Reno River**

105

106 The synergic role of fast subsidence and large sedimentary input have produced very high
107 sedimentation rates and frequent changes in the fluvial drainage framework of the central part
108 of the eastern Po plain (Fig. 1). The evolution of the river network can be reconstructed and
109 dated in great detail, through the correlation of the stratigraphic sedimentological evidence
110 with compositional data (Lugli et al., 2007) and a large amount of historical information and
111 accurate ancient maps (e.g. Bondesan 1989; Caputo et al., 2015).

112 In the late Middle Age, the Reno River was neither able to reach the Adriatic Sea nor to
113 directly flow into the Po River, which was running about 10 km to the north of the study area.
114 At that time the Reno River was mostly feeding a large paludal area and only at the end of the
115 18^o century it was successfully forced to reach the sea, through an abandoned southern
116 distributary channel of the Po River. The diversion point is located just to the southwest of the
117 investigated site (Fig.1). The investigated sector of the channel-levee system was already built
118 in its present form at the beginning the 15th century C.E. and its depositional morphology is
119 still recognizable today. It consists of a concave belt oriented SW-NE (the former channel),
120 bordered by two marginal ridges (the levees) rising up to 4-5 m above the surrounding
121 floodplain. The topographic gradients created by the channel-levee ridge had a major role in
122 the coseismic liquefaction dynamics, which was emphasized by lateral spreading phenomena
123 (Papathanassiou et al. 2012).

124 The old Reno River channel-levee system was deposited on top of an alluvial sedimentary
125 succession that was thoroughly investigated by boreholes, geotechnical and geognostic
126 surveys. The shallow sequence (Calabrese et al., 2012) can be divided into three main units
127 (A, B, C), from the top to the bottom (Fig. 2):

128 - unit A, Recent channel-levee unit consisting of medium sand belts (channels) and alternate
129 fine sand-mud bodies (levees and proximal crevasse splays), spanning from the surface to

130 about -13 m below the old channel ridge and -5 to - 6 m below the present-day floodplain; its
131 base has been radiocarbon dated to a numerical age of 1450-1581 C.E.;

132 - unit B, Holocene paludal unit, consisting of floodplain mud and peat, with isolated channel
133 and crevasse-splay sand bodies; this unit is 6 to 10 m-thick and was deposited starting roughly
134 since the beginning of the Holocene;

135 - unit C, latest Pleistocene floodplain unit, consisting of floodplain mud, and channel and
136 levee sand bodies deposited during and following the last glacial maximum.

137 The earthquake shaking produced an array of fractures roughly parallel to the old river ridge
138 that were exposed for a few months by digging a trench opened a few weeks after the main
139 shock. The sedimentary sequence exposed in the trench (Caputo et al., 2012) belongs to the
140 upper part of the Recent channel-levee system of the unit A and consists of four main
141 depositional facies associations (Fig. 2):

142 A1) distal levee to proximal alluvial plain silts and silty clays, with graded fine-sand overbank
143 beds, which are partially amalgamated by bioturbation, contain root structures and show
144 pedogenetic alteration, traces of agricultural activity and ceramic fragments;

145 A2) proximal levee sands and sandy silts, with direct gradation and tractive lamination
146 structures;

147 A3) channel sediments consisting of medium sand, showing festoon cross stratification. The
148 sand contains argillaceous rip-up clasts, rounded armored mud balls, wood and brick
149 fragments;

150 A4) channel sands slightly older than A3, that were intercepted by drilling at the base of the
151 trench (depth 6.8-7.5 m).

152 The above sequence is cross cut at high angle by several dikes which represent extension
153 fractures infilled by sands injected upward from the trench bottom. Some of them reach the
154 topographic surface and extend horizontally outside the trench for tens of meters, while others

155 stop below the ploughed layer (about 0.5-1 m deep); the latter have been associated with the
156 1570 Ferrara earthquake (Caputo et al., 2012).

157

158

159 **4. Materials and methods**

160

161 The sampling of sand has been done in a trench dug immediately after the seismic event,
162 which allowed the detailed observation of the fluvial sedimentary sequence across the Reno
163 River down to the depth of about 6 m (Fig. 2). The sediments consist of cross-bedded sands
164 from the paleo-channel of the Reno River and the laminated sand-mud levee deposits cut by
165 the liquefaction sand dikes. We sampled also cores from deeper sand horizons crossed by
166 drillings down to the maximum depth of 50 m. A total of 41 sand samples were collected and
167 analyzed: - 17 samples from the five dikes (named D 3, 4, 5, 6 and 7 in the trench section
168 shown in Fig. 2), each dike sampled at different depths; - 4 samples from the modern sands of
169 the present-day Reno River; - 10 samples from the levee (unit A1-A2) and channel fill (A3) of
170 the paleo Reno River; - 4 samples from paleo-channel sands drilled at the bottom of the trench
171 (unit A4), - 6 samples from cores outside the trench from unit B (borehole S2, 8.20 to 10.45 m
172 depth and borehole S3, 6.90 to 9.60 m depth) and the lower sand layer dating back to the
173 uppermost Pleistocene (borehole S10, 22.50 to 24.50 m depth, unit C). Sample location is
174 shown in Fig. 2.

175 Grain-size analyses were performed using standard techniques: mechanical sieving for the
176 sandy fraction and hydrometer analysis for fine-grained sediments. Sand samples consisting
177 of a few hundreds of grams were washed with dilute H₂O₂ to remove organic matter and were
178 air dried and mechanically sieved for granulometric and compositional analyses. The result of
179 grain size analyses for most of the samples is a mean value of multiple bands that are a few
180 millimeters to centimeters in thickness, as sampling encompassed many of these vertical

181 features (see sedimentological description).
182 For the compositional analyses, two sub-samples were prepared for each samples: the whole
183 sandy fraction (for qualitative observations) and the fine sand fraction (0.125–0.250 mm) for
184 point counting. The necessity to analyze the fine sand fraction was dictated by the lack of
185 medium-coarse sand at some of the sampling sites and for comparison with the same grain-
186 size fraction used in Lugli et al. (2007). Sands were impregnated in epoxy resin under vacuum,
187 thin-sectioned, and stained for carbonate identification. Point counting under transmitted light
188 microscopy was performed on the 0.125–0.250 mm fraction, according to the Gazzi-
189 Dickinson method (Zuffa, 1985; Weltje, 2002). At least 300 grains were point counted for
190 each section to achieve modal composition. Results of point counting are presented in Table 1.
191 Components not related to the original sand composition, such as authigenic carbonate
192 nodules, penecontemporaneous shell fragments, soil and organic fragments were excluded
193 from the final calculations.

194

195

196 **5. Results**

197

198 *5.1 Sedimentology of the sand blows*

199

200 The coseismic sand dikes represent vertical straight, planar or curved extension features
201 crosscutting the sequence at high angles from the base of the trench to the topographic surface
202 with a vertical extension of at least 5 m. In several cases (dikes D 5, 6, 7) they stop 1 m or a
203 few decimetres below the surface, but the main fracture may have reached the surface
204 elsewhere. The width of the fractures varies from a few centimetres to about 30 cm. Most
205 fractures are single, but tapering and bifurcation are also present (Fig. 3 and 4). Some fracture

206 margins are closely spaced locally and are partially filled by muddy fragments from the host
207 sediment (Fig. 3).

208 The sand injected into the fractures shows complex sedimentary structures similar to those
209 described by Nichols et al (1994) and Hurst et al. (2011; see also references therein). The
210 most common feature is a distinct banding, that ranges in thickness from 0.3 to 3 cm (Fig. 5),
211 and can be longitudinal to the dike length, or perpendicular to the dike margins (Figs. 3, 4, 5).

212 The bands oriented parallel to the dike are bounded by sharp contacts marked by thin clay
213 veneers and are defined by differences in grain size and grain alignment. The multiple sets of
214 graded layers that form the banding may show variable thickness along the dikes and some
215 bands scoured into adjacent layers (Fig. 3 and 4). The largest fractures are filled by massive
216 sand which graded along the vertical fissures (Fig. 5) and show an internal stratification
217 consisting of multiple superimposed concave fine-grained veneers (Fig. 3). We observed both
218 direct and inverse vertical grading of the sand from medium sand to mud. Similar well-
219 laminated structures are observed in sand volcanoes that formed on the top of the fractures in
220 many of the liquefaction sites around San Carlo (Fig. 6).

221

222 *5.2 Grain-size distribution*

223

224 Results of grains size analysis are reported in Fig 7. The content of sand, silt and clay for all
225 samples is shown in the triangular plot of Fig. 8. The samples range from almost pure sands to
226 silt, with a content of clay less than 20%. Samples from the levee facies are the finest, made
227 up of coarse silt to very fine to fine sands. Samples from the paleo-channel and from deeper
228 layers are predominantly medium and medium-coarse grained sands. The dikes consist mainly
229 of very fine to fine and medium sands. In four samples the amounts of coarse-grained sand is
230 higher than 10 %. One dike sample is made up of silt. In all dikes the amount of clay is less
231 than 10 %. The grain-size distribution along the same dike shows no systematic trends, as

232 samples located nearby each other may have different grain-size. This is shown by the
233 diagram of Fig 9 that plots the mean diameter for each dike at different depths: dike D 3 is
234 characterized by a slight grain size increase from the lower portion to the top, while an
235 opposite trend is observed in dike 5.
236 Sorting of all sands is moderate to poor and for dikes ranges from 1.22 to 2.46.

237

238 *5.3 Sand Composition*

239

240 *5.3.1 The modern Reno River fluvial sands.*

241 Among the examined samples, the sands from the modern Reno River are the most
242 lithoarenitic; they are made up of quartz (ranging from 29.7 to 35.19%, Table 1), feldspars
243 (15.2 -21.7%) and sedimentary fine-grained siliciclastic and carbonate lithics. Shales are the
244 dominant lithic grains (12.4 to 18.6%); they are well lithified, well rounded, with an evident
245 iso-orientation of clay minerals, and for these characters they appear to have a detrital origin,
246 derived from older pelitic successions of the Northern Apennines. Minor intrabasinal muddy
247 components consisting of penecontemporaneous rip-up clasts have also been observed. Sands
248 of the modern Reno River are well distinguishable from the other rivers of the Po plain, as
249 defined by Lugli et al. (2007).

250

251 *5.3.2 The paleo Reno River fluvial sands*

252 The sand samples from the paleo-Reno levee (unit A1-A2) and channel fill (A3) are quite
253 homogeneous in composition (Fig. 10 a, b), slightly impoverished in lithic fragments
254 compared to the modern Reno River sands. The amount of quartz ranges from 29.7 to 37.7%.
255 Feldspars (both plagioclase and K-feldspar) vary from 18.1 to 23.7%. Fine-grained lithics are
256 mainly sedimentary, made up of micritic and sparitic limestones (from 9.4 to 17.0%) and
257 siltstones and shale (14.4 to 20.4%). Metamorphic lithics and cherts are minor components.

258 The composition of older channel sands (Unit A4), shows quartz content ranging from 28,8 to
259 39.6%, feldspars from 20.1 to 26.6%, siltstones and shale vary from 14.5 to 23%, carbonates
260 from 21.3 to 23.7%.

261

262 *5.3.3 The sand dikes*

263 The sands filling the dikes show relatively homogeneous composition (Fig. 10d) with one
264 exception. Total quartz range from 31.2 to 42.2%, feldspars from 16.3 to 24.9%. Carbonate
265 lithics vary from 22.3 to 30.2%; siltstones and shales range from 11.8 to 18.4%. Only one
266 sample (no. 23) from the deepest portion of dike 3, shows higher quartz and feldspar content
267 and is very low in siliciclastic lithics. Sands from single dikes at different depths show minor,
268 non-systematic, compositional variations, mainly due to quartz and lithic fragments variations
269 (see Fig. 9).

270

271 *5.3.4 The older sands: Holocene (unit B) to Pleistocene (unit C)*

272 The core fluvial sands in the subsurface at depths from 7 to 10 m (Holocene) and from 22 to
273 24 m (Pleistocene in age) are rich in quartz and feldspar and metamorphic rock fragments
274 (Fig.10c). Quartz range from 36.7 to 54.0%; feldspars vary from 19.7 to 28.6%; siltstones and
275 shales are less than 11% and carbonate lithics range from 16 to 29.1%. Coarse-grained
276 metamorphic rock fragments are also present.

277

278 *5.3.5 Compositional fields*

279 Data from modal analyses are reported in the classification diagram Q+F (quartz+feldspars),
280 L (siliciclastic fine-grained lithics), C (carbonate lithics) of Fig. 11, in which compositional
281 fields of others fluvial sands in the Po plain are also reported (Lugli et al 2007).

282 The examined sands are characterized by well defined fields and show a clear trend from
283 lithoarenitic to quartz-feldspar-rich compositions. In detail the sands from the modern Reno

284 River are the most lithoarenitic, with shales as the dominant lithic type. Sands are well
285 distinguishable from the other rivers of the Po plain, as defined by Lugli et al. (2007). The
286 sand from the paleo-Reno channel fill show composition slightly enriched in quartz and
287 feldspars and impoverished in lithic fragments compared to the modern Reno River sands. A
288 similar composition characterizes also sands at shallow depth (unit A4, 6.8-7.5 m depth). In
289 the modern and paleo Reno river sands the lithic fragments derive mostly from the erosion of
290 sedimentary carbonate and terrigenous successions.

291 Composition of dike sands clearly overlap that of the paleo-Reno river sands down to the
292 depth of 7.5 m. Older Holocene sands coming from layers deeper than 8 m and the
293 Pleistocenic sands (unit C) differ in composition and show an higher quartz-feldspar content.
294 A similar enrichment in quartz and feldspars in the Pleistocene fluvial sands, compared with
295 the present-day sands, was noted by Lugli et al. (2007) for the fluvial sediments of the Po
296 alluvial plain. This shifting composition back in time was interpreted as a consequence of the
297 different climatic weathering condition that occurred during the last glacial stage. The strong
298 denudation, erosion and accelerated transport were probably responsible of promoting the
299 survival of feldspar grains.

300

301 *5.3.6 Grain-size influence on sand composition*

302 As the counting technique here adopted (Zuffa, 1985) is especially designed to minimize the
303 dependence of the analysis from the grain-size, we plotted the mean diameter and the percentage of
304 significant types of grains (quartz and feldspars, shales, carbonates) in order to verify the reliability
305 of the point counting analyses. Plot of Fig. 12 shows no correlation between composition and grain-
306 size of sands. These results suggest that disintegration, microfracturing or erosion of most erodible
307 grains, such as shales, due to the abrasive flow of sand grains was not responsible of significant
308 compositional variation.

309

310

311 **6. Discussion**

312

313 In our study, texture and composition characteristics provide important constrains for source
314 layer indentification in liquefaction processes and flow regime.

315 Although there is currently no unequivocal evidence that texture in sand dikes (i.e. lamination,
316 clay content, alignment of platy and elongate grains) may be indicative of a particular flow
317 regime (Hurst et al., 2011), the diverse sedimentary features coexisting within the same dike,
318 are probably related to the multiple rythmic opening and closing of the fracture borders that
319 may have lasted for several minutes. The sedimentary features suggest that the fractures were
320 rhythmically injected and filled of slurry sand and mud during the compression pulses end
321 emptied by the rushing of the slurry back down deep into the fractures during the extension
322 peak. These alternate flows, together with the sequential opening of various fractures in
323 different area, may account for the presence of both inverse and direct grading of the sand
324 filling different portion of the same dike and for the concave stratification of the dikes.

325 Unfortunately this phenomenon was not observed directly in May 2012, but similar examples,
326 although of much larger magnitude, were filmed during the M 9.0 Tohoku great earthquake in
327 Japan (see Great Japan Earthquake, 2011, www.youtube.com/watch?v=TzlodnjPAuc).

328 The pulse mechanism of sand blows is also supported by the well stratified structure of the
329 sand volcanoes that formed on the top of the fractures in many of the liquefaction sites around
330 San Carlo (Fig. 6) and elsewhere, a feature described also by Rodríguez-Pascua et al. (2015).

331 These volcanoes are up to a few tens of centimeters high and show several centimetic to
332 millimetric alternance of graded laminae consisting of sand and mud (Fig. 6).

333 The grain-size distribution of the sands filling dikes clearly overlaps that of sands at dephts of 6.8-
334 7.5 meters, and in deeper layers. Grain-size distribution of examined dikes show a good agreement
335 with the grain-size characteristic reported in the literature for sands ejected during earthquakes in

336 California or Japan (Kishida,1970; Figueroa et al.,1995). In particular, the amount of clay less than
337 10% fits with other case histories that show that only sand with a low natural clay content are
338 susceptible to liquefaction. Tokimatsu and Yoshimi (1983) documented 70 cases in Japan resulting
339 from 10 separate earthquakes that show a cut-off for liquefaction susceptibility at a clay content of
340 about 15-10%.

341 The composition adds an important constraint in identifying the source layer. Composition of the
342 sand filling the dikes show close similarity with the composition of the sand layer located at a
343 depth from 6.8 to 7.5 metres (Unit A4), while clearly differ from deeper sands which are richer in
344 quartz and feldspar and poorer in sedimentary lithic fragments. These data clearly indicate a
345 relatively shallow source for the blowouts.

346 About the relatively shallow depth of the source layer, it is known that the liquefaction
347 resistance of a soil deposit increases with depth as the effective overburden pressure increases.
348 For this reason, sand deposits deeper than about 15 m are rarely observed to liquefy
349 (Krinitzsky et al. 1993). Particle cementation, not observed in the examined dike sands, is also
350 an important factors and layers older than the Holocene are usually not prone to liquefaction
351 (Youd and Perkins 1978), perhaps due to a weak cementation at the grains.

352 Regarding the possibility that selective mechanism due to flux variation may have influenced
353 the sand composition, our data seem to indicate that no major variation was induced by
354 liquefaction phenomena. This is probably the result of the point counting technique which
355 seems to successfully reduce the effect of grain size over composition.

356 Finally, an interesting point concerns the enrichment in quartz and feldspars in the relatively
357 shallow sands of unit B deposited by the Reno River in the Holocene (pre 16th century C.E.), which
358 are similar to the deeper Pleistocene sands (unit C). This could be due to partial recycling of sands
359 deposited during the last glacial maximum at about 20 ka. Another possibility is that the drainage
360 network was different from that of today, as suggested by Ravazzi et al. (2013), and those sand may
361 have been deposited by another river, the Enza, which is today flowing much further to the west.

362

363 **6. Conclusions**

364

365 The study of the sands injected in the San Carlo area (Ferrara) during the Mw 6.1 earthquake,
366 and the comparison of their texture and composition with those of buried fluvial sediments as
367 deep as 20 m provided us with clues about the emplacement mechanisms and the source
368 layers identification.

369 The sands from the dikes show a composition compatible with that of the recent shallow
370 sands deposited by the Reno River. These sands clearly differ from deeper sands (at depth of
371 more than 8 m), which are richer in quartz and feldspar and poorer in sedimentary lithic
372 fragments as a consequence of their deposition during the last glacial maximum and later
373 reworking.

374 Composition and fabric characteristics, such as grain-size distribution and clay content,
375 indicate that liquefaction processes affected mainly sand layers at depth of 6.8-7.5 m, a
376 relatively shallow source for the blowouts. Pulsations in the flow during shaking appear to be
377 responsible for the concave and vertical layering within the dikes, normal and inverse
378 gradation along the dikes and only modest petrographic compositional variations within
379 individual dikes.

380 Our results show that selective mechanisms due to flux variation have not influenced the sand
381 composition and thus petrographic point-counting methodology may be successfully applied
382 to trace back the source sand layers of ancient blowouts.

383

384 **Acknowledgements**

385 We are indebted with the Municipality of Sant'Agostino and Regione Emilia Romagna for
386 supporting the trench investigation. We thank D. Castaldini, G. Bertolini, C. Fioroni and M.
387 Bertacchini help in sampling and E. Carnevali for grain size analyses.

388

389

390 **References**

- 391 Amorosi, A., Pavesi, M., Ricci Lucchi, M., Sarti, G., Piccin, A., 2008. Climatic signature of cyclic
392 fluvial architecture from the Quaternary of the central Po Plain, Italy. *Sedimentary Geology*,
393 209, 58–68.
- 394 Argnani, A., Fontana, D., Stefani, C., Zuffa, G.G., 2004. Late Cretaceous carbonate turbidites of the
395 northern Apennines: Shaking Adria at the onset of Alpine collision. *Journal of Geology*, 112 (2),
396 251-259.
- 397 Arribas, J., Tortosa, A., 2003. Detrital modes in sedimenticlastic sands from first-order streams of
398 the Iberian Range, Spain: The potential for sand generation of different sedimentary rocks.
399 *Sedimentary Geology*, 159, 275- 303.
- 400 Bettelli, G., De Nardo, M.T., 2001. Geological outlines of Emilia Apennines (Italy) and
401 introduction to the rock units cropping out in the areas of landslides reactivated in the 1994–1999
402 period. *Quaderni di Geologia Applicata*, 8(1), 7–26.
- 403 Bondesan, M. (1989). *Evoluzione geomorfologica e idrografica della pianura ferrarese*, Terre ed
404 Acqua, Corbo Editore, 14-20.
- 405 Basu, A., Schieber, J., Patranabis–Deb, S., Chandra Dhang, P., 2013. Recycled detrital quartz
406 grains are sedimentary rock fragments indicating unconformities: examples from the
407 Chhattisgarh Supergroup, Bastar craton, India. *Journal of Sedimentary Research*, 83, 368–
408 376.
- 409 Burrato, P., Vannoli, P., Fracassi, U., Basili, R., Valensise, G., 2012. Is blind faulting truly
410 invisible? Tectonic-controlled drainage evolution in the epicentral area of the May 2012,
411 Emilia-Romagna earthquake sequence (northern Italy). *Ann. Geophys.* 55 (4), 525–531.
412 <http://dx.doi.org/10.4401/ag-6182>.

- 413 Calabrese, L., Martelli, L., Severi, P., 2012. Stratigrafia dell'area interessata dai fenomeni di
414 liquefazione durante il terremoto dell'Emilia (maggio 2012). 31° Conv. Naz. GNGTS,
415 Potenza, November 20–22, (2), 119–126.
- 416 Caputo R., Iordanidou K., Minarelli L., Papathanassiou G., Poli M.E., Rapti-Caputo D.,
417 Sboras S., Stefani M., Zanferrari A., 2012. Geological evidence of pre-2012 seismic
418 events, Emilia-Romagna, Italy. *Annals of Geophysics*, 55, 743-749.
- 419 Caputo, R., Pellegrinelli, A., Bignami, C., Bondesan, A., Mantovani, A., Stramondod, S.,
420 Russo, P., 2015. High-precision levelling, DInSAR and geomorphological effects in the
421 Emilia 2012 epicentral area. *Geomorphology* 235, 106–117
- 422 Chang, W.-J., Ni, S.-H., Huang, A.-B., Huang, Y.-H., Yang, Y.-Z., 2011. Geotechnical
423 reconnaissance and liquefaction analyses of a liquefaction site with silty fine sand in
424 Southern Taiwan. *Engineering Geology* 123, 235–245.
- 425 Chen, L., Hou, L., Cao, Z., Yuan, X., Sun, R., Wang, W., Mang, F., Chen H. Dong, L., 2008.
426 Liquefaction investigation of Wenchuan earthquake. The 14th World Conference on
427 Earthquake Engineering, October 12-17, 2008, Beijing, China.
- 428 Critelli, S., Arribas, J., Le Pera, E., Tortosa, A., Marmaglia, K.M., Latter, K.K., 2003. The recycled
429 orogenic sand provenance from an uplifted thrust belt, Betic Cordillera, southern Spain. *Journal*
430 *of Sedimentary Research*, 73, 72–81.
- 431 Figueroa, J. L., Saada, A. S., Liang, L., 1995. Effect of the Grain Size on the Energy Per Unit
432 Volume at the Onset of Liquefaction. *Proceedings: 3rd International Conference on Recent*
433 *Advances in Geotechnical Earthquake Engineering and Soil Dynamics*, 1, 197-202
- 434 Garzanti, E., Vezzoli, G., Andò, S., 2011. Paleogeographic and paleodrainage changes during
435 Pleistocene glaciations (Po Plain, Northern Italy). *Earth Science Reviews*, 105 (1-2), 25-48.
- 436 Hurst A., Scott A., Vigorito M., 2011. Physical characteristics of sand injectites. *Earth-Science*
437 *Reviews*, 106, 215–246.
- 438 Johnsson, M.J., Stallard, R.F., and Lundberg, N., 1991. Controls on the composition of fluvial sands

439 from a tropical weathering environment; sands of the Orinoco River drainage basin, Venezuela
440 and Colombia. Geological Society of America Bulletin, 103, 1622–1647.

441 Kishida, H., 1970. Characteristics of Liquefaction of Level Sandy Ground During the Tokachioki
442 Earthquake. Soils and Foundations, 10(2), 103-111:

443 Lugli S., Marchetti Dori S., Fontana D. 2007. Alluvial sand composition as a tool to unravel
444 the Late Quaternary sedimentation of the Modena Plain, northern Italy. In: Arribas, J.,
445 Critelli, S., Johnsson, M.J. (Eds.), Sedimentary Provenance and Petrogenesis: Perspectives
446 from Petrography and Geochemistry. Geological Society of America Special Paper, 420,
447 57-72.

448 Nichols, R.J., Sparks, R.S.J., Wilson, C.J.N., 1994. Experimental studies of the fluidization of
449 layered sediments and the formation of fluid escape structures. Sedimentology ,41, 233-
450 253.

451 Papathanassiou, G., Mantovani, A., Tarabusi, G., Rapti, D., Caputo R., 2015. Assessment of
452 liquefaction potential for two liquefaction prone area considering the May 20, 2012 Emilia
453 (Italy) earthquake. Eng. Geol., 189, 1-16.

454 Pieri, M., Groppi, G., 1981. Subsurface geological structure of the Po Plain, Italy, C.N.R.,Progetto
455 Finalizzato Geodinamica, Publ. 414, 1-13.

456 Pondrelli, S., Salimbeni, S., Perfetti, P., Danecek, P., 2012. Quick regional centroid moment tensor
457 solutions for the Emilia 2012 (northern Italy) seismic sequence. Annals of Geophys, 55(4), 615-
458 621.

459 Ravazzi, C., Marchetti, M., Zanona, M., Peregoc, R., Quirino, T., Deaddis, M., De Amicis, M.,
460 Margaritora, D., 2013. Lake evolution and landscape history in the lower Mincio River valley,
461 unravelling drainage changes in the central Po Plain (N-Italy) since the Bronze Age. Quaternary
462 International, 288-195-205.

463 Ricci Lucchi F., 1986. Oligocene to Recent foreland basins Northern Apennines. I.A.S., Special
464 Public. 8, Blackwell, 105-139.

465 Rodríguez-Pascua, M.A., Pablo G. Silva, P.G., Perez-Lopez, R., Giner-Robles, J.L., Martín-
466 Gonzalez, F., Del Moral, B., 2015. Polygenetic sand volcanoes: On the features of liquefaction
467 processes generated by a single event (2012 Emilia Romagna 5.9 M w earthquake Italy).
468 Quaternary International 357, 329-335.

469 Tokimatsu., K., Yoshimi, Y., 1983. Empirical Correlation of Soil Liquefaction Based on SPT
470 N-Values and Fines Content. Soils and Foundations,. 23 (4), 56-74.

471 Weltje, G.J., 2002. Quantitative analysis of detrital modes: Statistically rigorous confidence regions
472 in ternary diagrams and their use in sedimentary petrology. Earth-Science Reviews, 57, 211–253.

473 Weltje, G.J., Von Eynatten, H., 2004. Quantitative provenance analysis of Sediments. Review and
474 outlook. Sedimentary Geology, 171, 1–11.

475 Youd, T.L., Perkins, D.M., 1978. Mapping liquefaction induced ground failure potential. Journal
476 of the Geotechnical Engennering Division, 443-446.

477 Zuffa, G.G., 1985. Optical analyses of arenites: Influence of methodology on compositional
478 results. In: Zuffa, G. (Ed.), Provenance of Arenites. Dordrecht/Boston/Lancaster, D.
479 Reidel Publishing Company, NATO ASI, 148, 165–189.

480

481

482 **Figure captions**

483

484 **Fig. 1.** Sketch map of the alluvial plain in the Emilia area affected by the May 2012
485 earthquakes (location of the two major epicenters are indicated with stars). The studied trench
486 is located at San Carlo, along an old Reno River channel abandoned as a result of the 18°
487 century diversion. Arrows indicate the river channel shift trends during the Holocene
488 (Modified from Burrato et al., 2012).

489

490 **Fig. 2.** a) Stratigraphic section of the old Reno river channel ridge at San Carlo. Depositional
491 facies and stratigraphic units (modified after Caputo et al. 2012 and Papathanassiou et al.,
492 2012). b) Stratigraphy and depositional units in the trench exposure along two walls (upper
493 section flipped) showing the sand dikes cutting the fluvial sequence. Sample location is also
494 reported. Modified after Caputo et al., 2012

495

496 **Fig. 3.** Dike D7 filled by laminated sand cutting through stratified proximal levee sand and
497 silt facies. The left side of the wall collapsed as a result of lateral spreading. Laminae within
498 the dike are highlighted by concave silt veneers suggesting multiple phases of sediment
499 settling by collapse of the sand column along the fracture. The fracture is locally filled by silty
500 clast originated by the mechanical crushing of the fracture borders (upper right). Location of
501 dike in the trench is shown in Fig. 2.

502

503 **Fig. 4.** Dike D5 cutting across bioturbated massive clayey silt. Note the cross cutting
504 relationships between the larger and smaller fracture which are also marked by a few oblique
505 fine-grained laminae (upper left). Sand in the larger dike is normally graded. Location of dike
506 in the trench is shown in Fig. 2.

507

508 **Fig. 5.** Distinct vertical lamination within dike D3. Single sand layers are graded and are
509 separated by thin fine-grained laminae. Layering is accentuated by differential weathering.
510 Location of dike in the trench is shown in Fig. 2.

511

512 **Fig. 6.** Ejected sand at San Carlo forming a volcano structure consisting of various laminated
513 sand layers. At least 6 sand/mud couplets are visible indicating multiple opening and closing
514 phases of the mother fracture.

515

516 **Fig. 7.** Cumulative grain size distributions of sands from the paleo Reno River levee and
517 channels, units B and C, and the dikes.

518

519 **Fig. 8.** Triangular plot showing the relative proportions of sand, silt and clay for the examined
520 samples.

521

522 **Fig. 9.** Variations in grain size (mean diameter), quartz+feldspars and shale contents in a
523 vertical profile along dikes 3 and 5.

524

525 **Fig. 10.** Photomicrographs of sands from the old Reno River channel (a), levee (b), Pleistocene
526 sands from unit C (c) and dike D3 (d). Transmitted light, crossed polars.

527

528 **Fig. 11.** Q+F, L, C diagram showing the composition of sands from dikes, recent and paleo
529 Reno River and from older units B and C. Composition of sands from the Modena plain
530 streams is also reported (Lugli et al., 2007). Q: quartz; F: feldspars; L: siliciclastic rock
531 fragments; C: carbonate rock fragments.

532

533 **Fig. 12** Plot showing the content of quartz+ feldspar vs the mean diameter for all the
534 examined samples. Note the lack of correlation between grain-size and composition. This
535 result is confirmed for the other compositional classes (not reported here).

536

537 **Table 1.** Results of petrographic modal analyses.

538

Figure 1

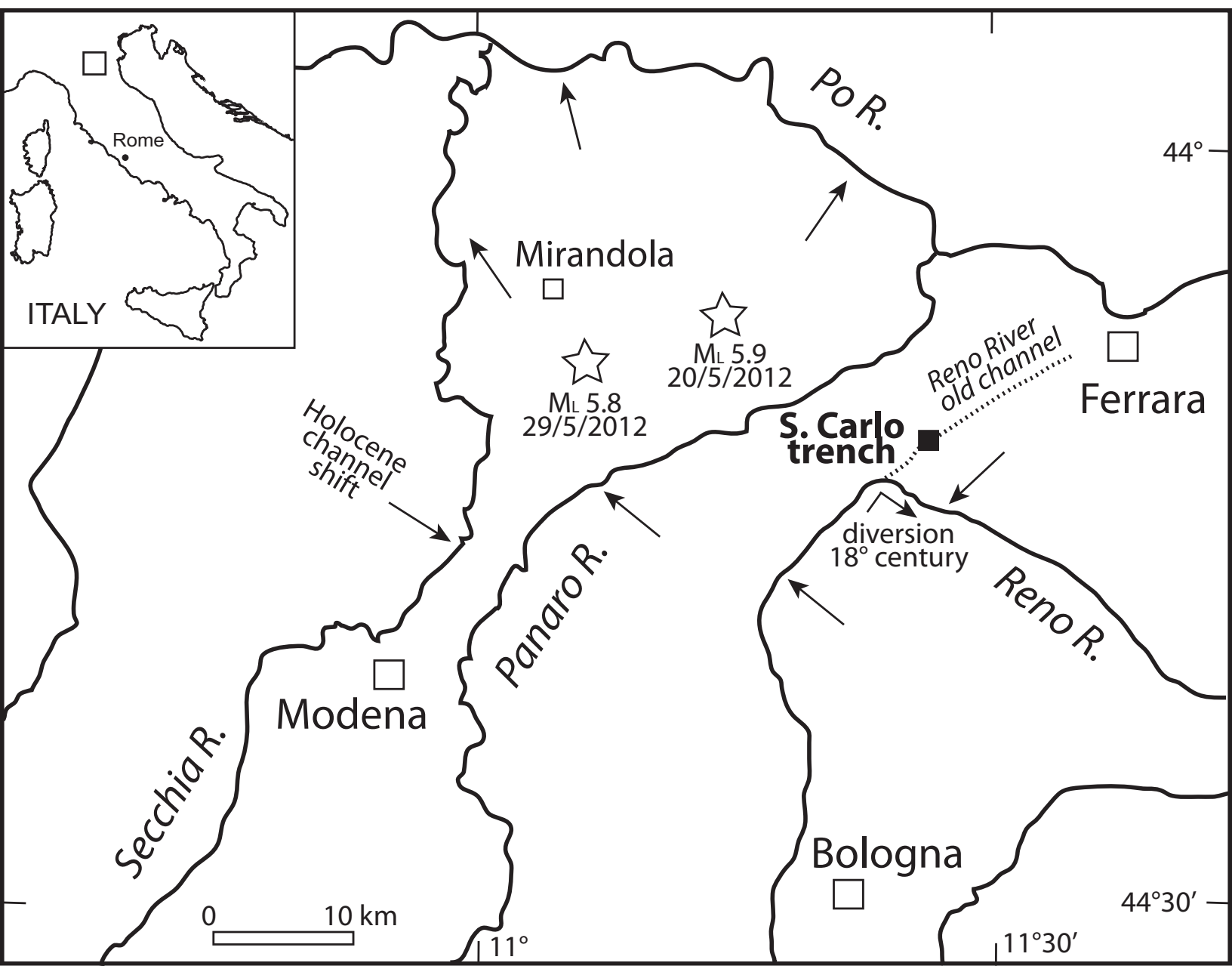


Figure 2

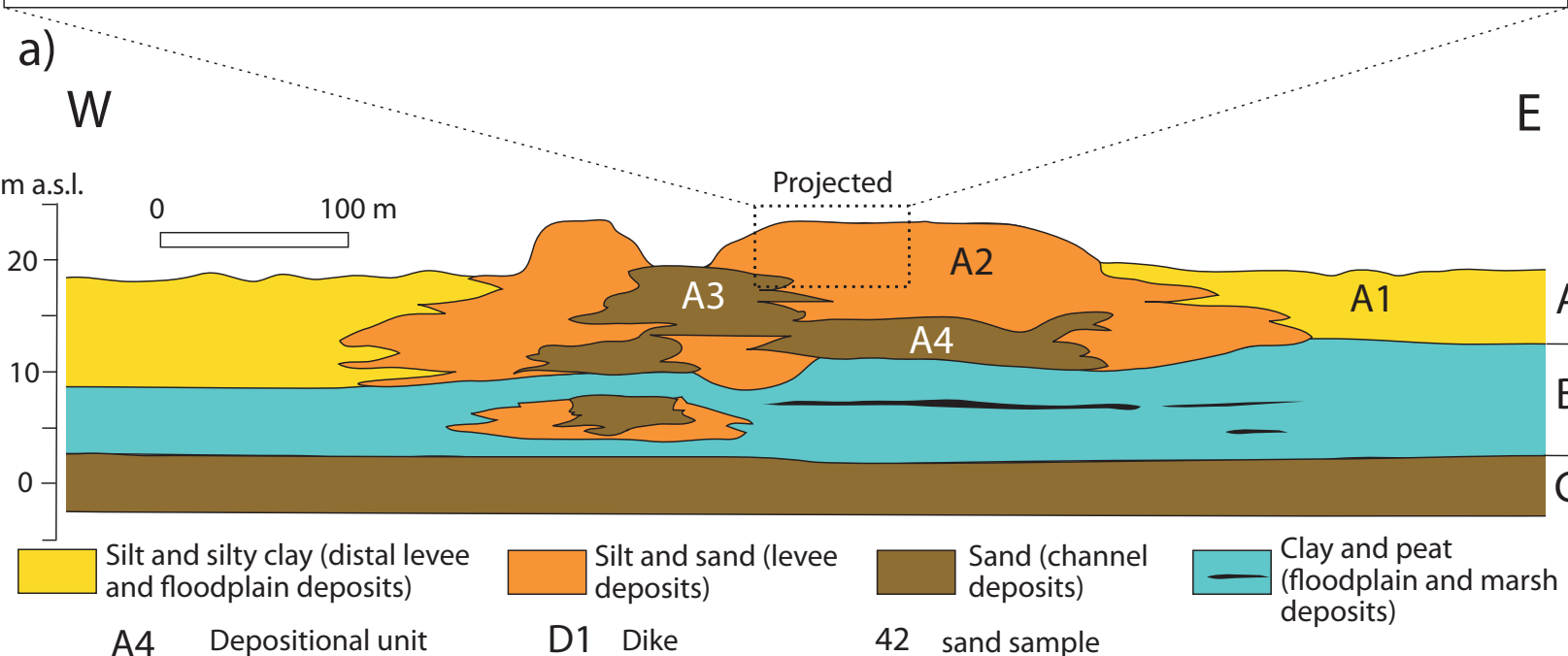
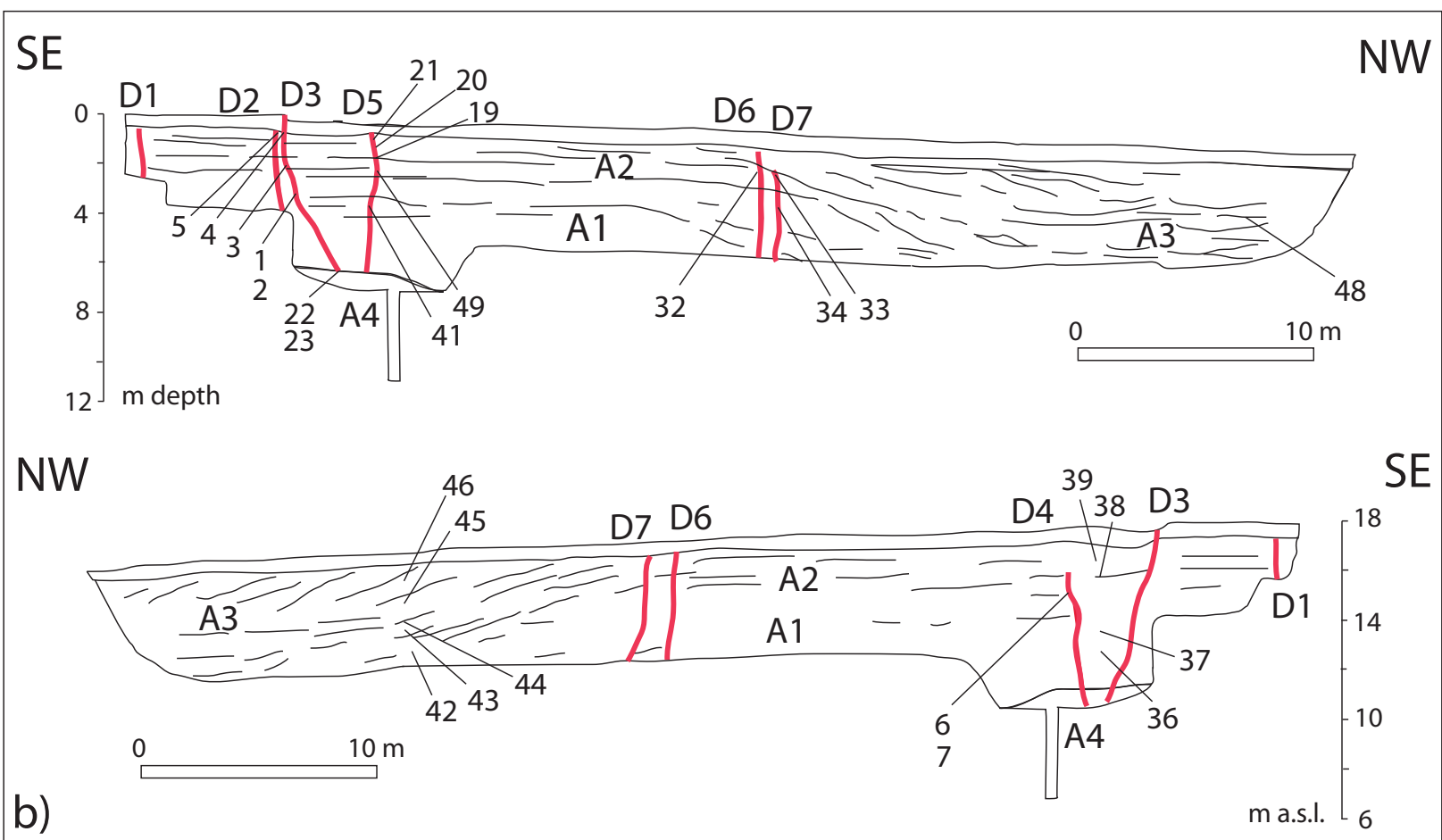


Figure 3
[Click here to download high resolution image](#)



Figure 4
[Click here to download high resolution image](#)

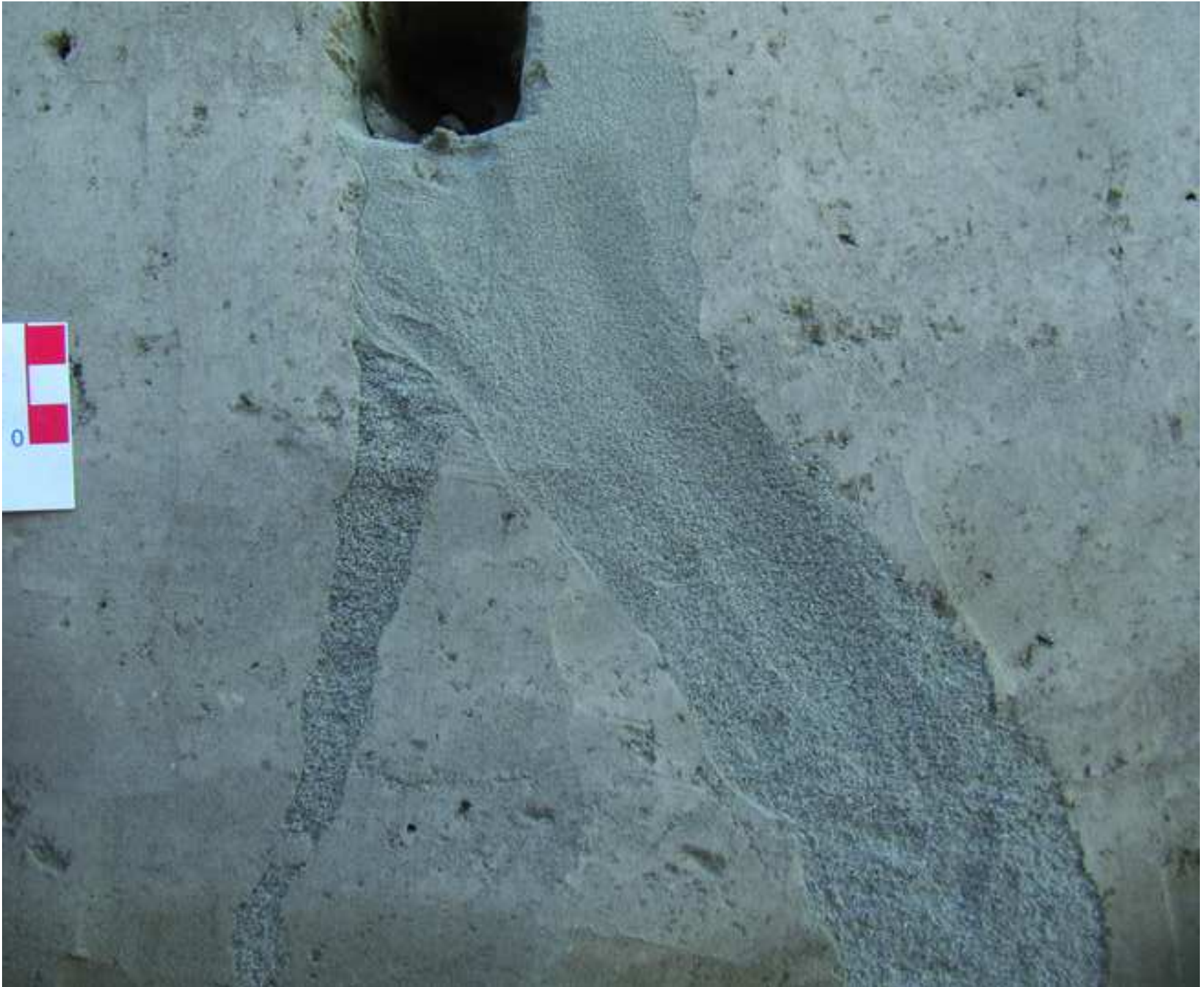


Figure 5
[Click here to download high resolution image](#)



Figure 6
[Click here to download high resolution image](#)



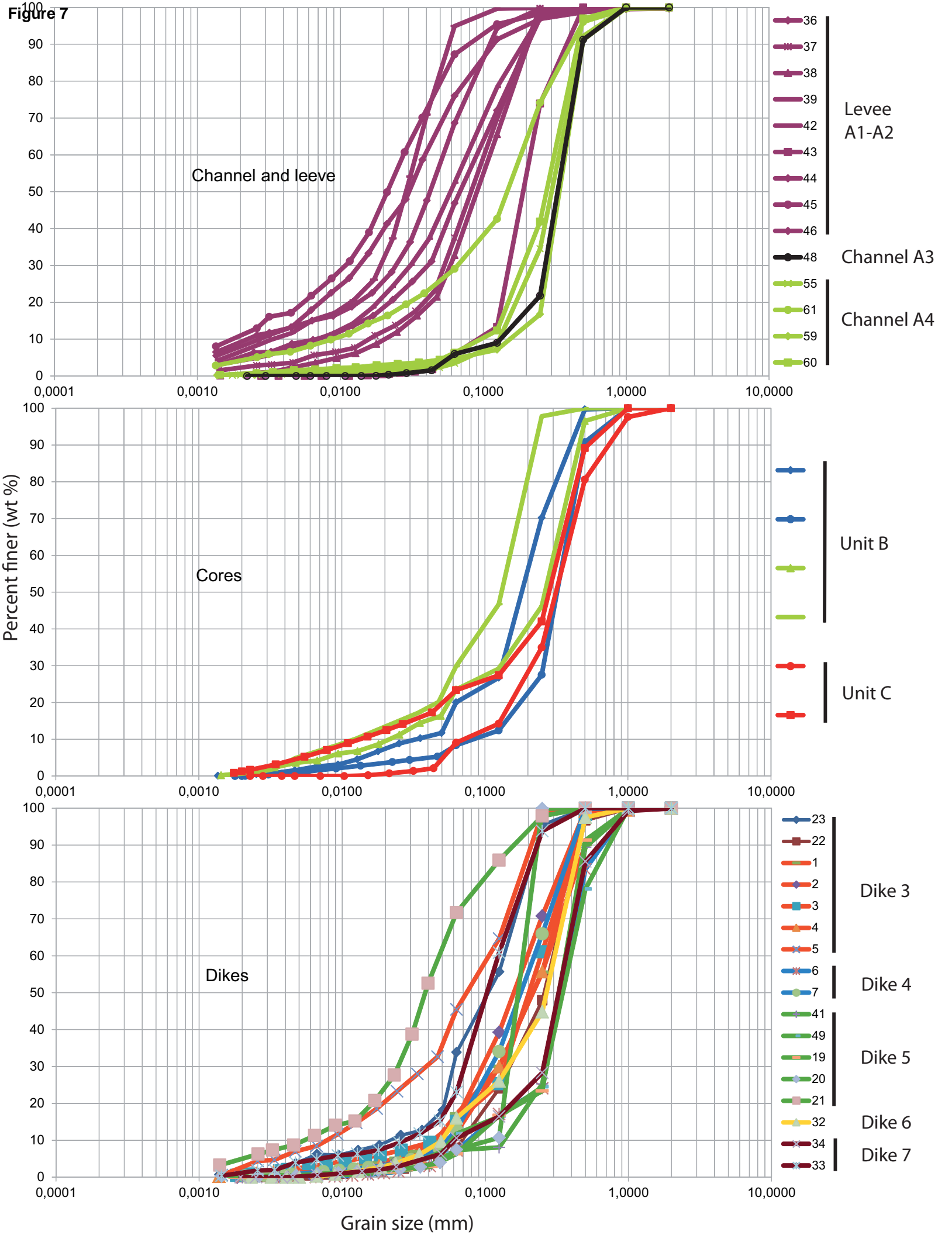
Figure 7

Figure 8

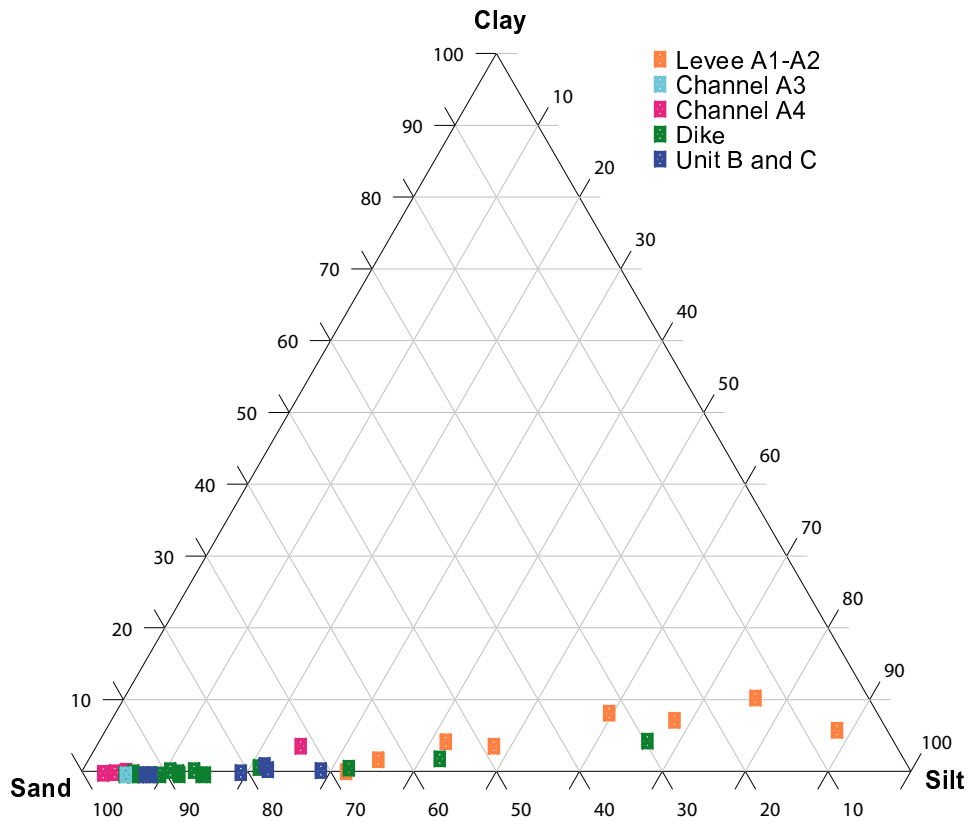


Figure 9

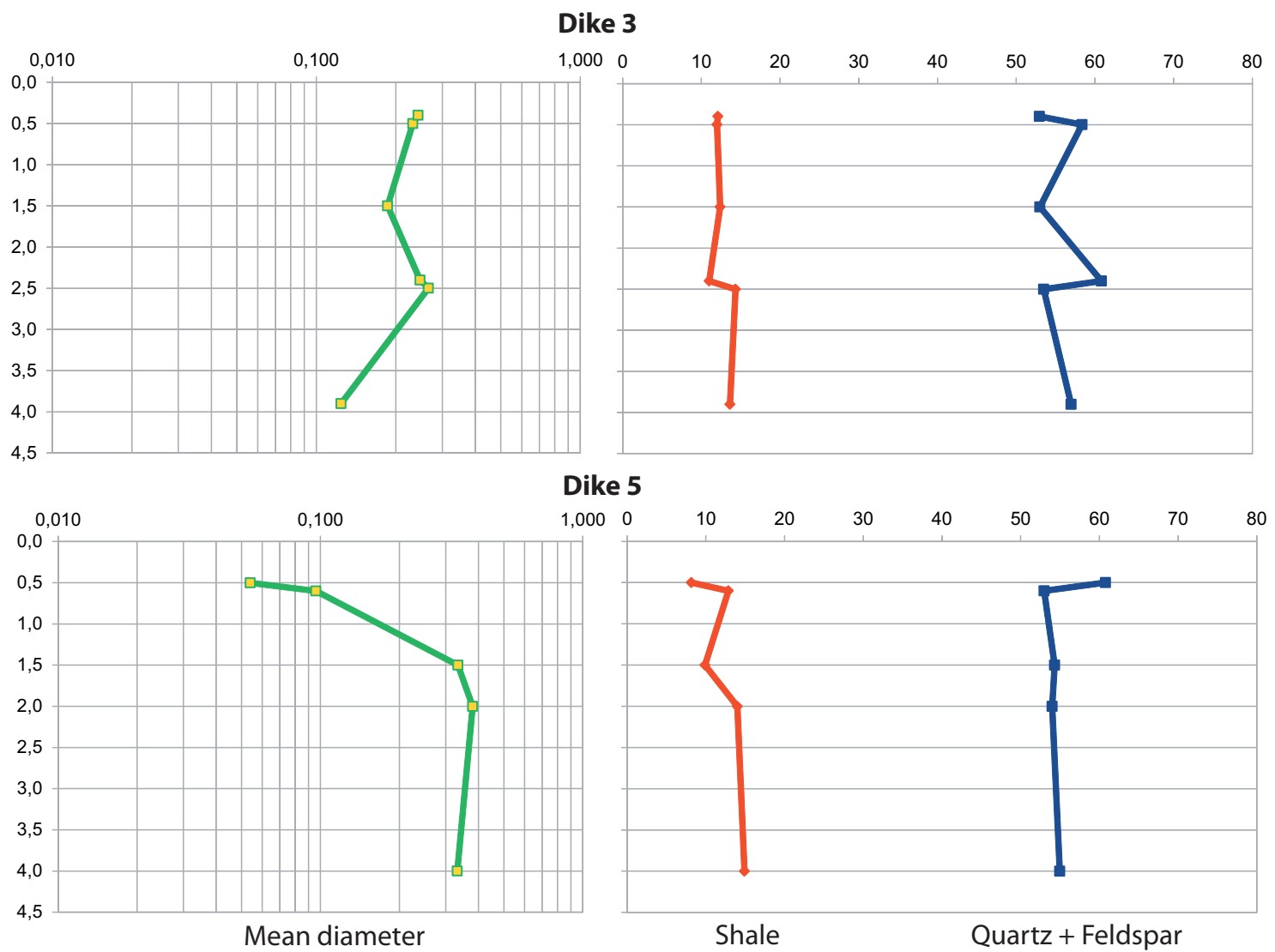


Figure 10
[Click here to download high resolution image](#)

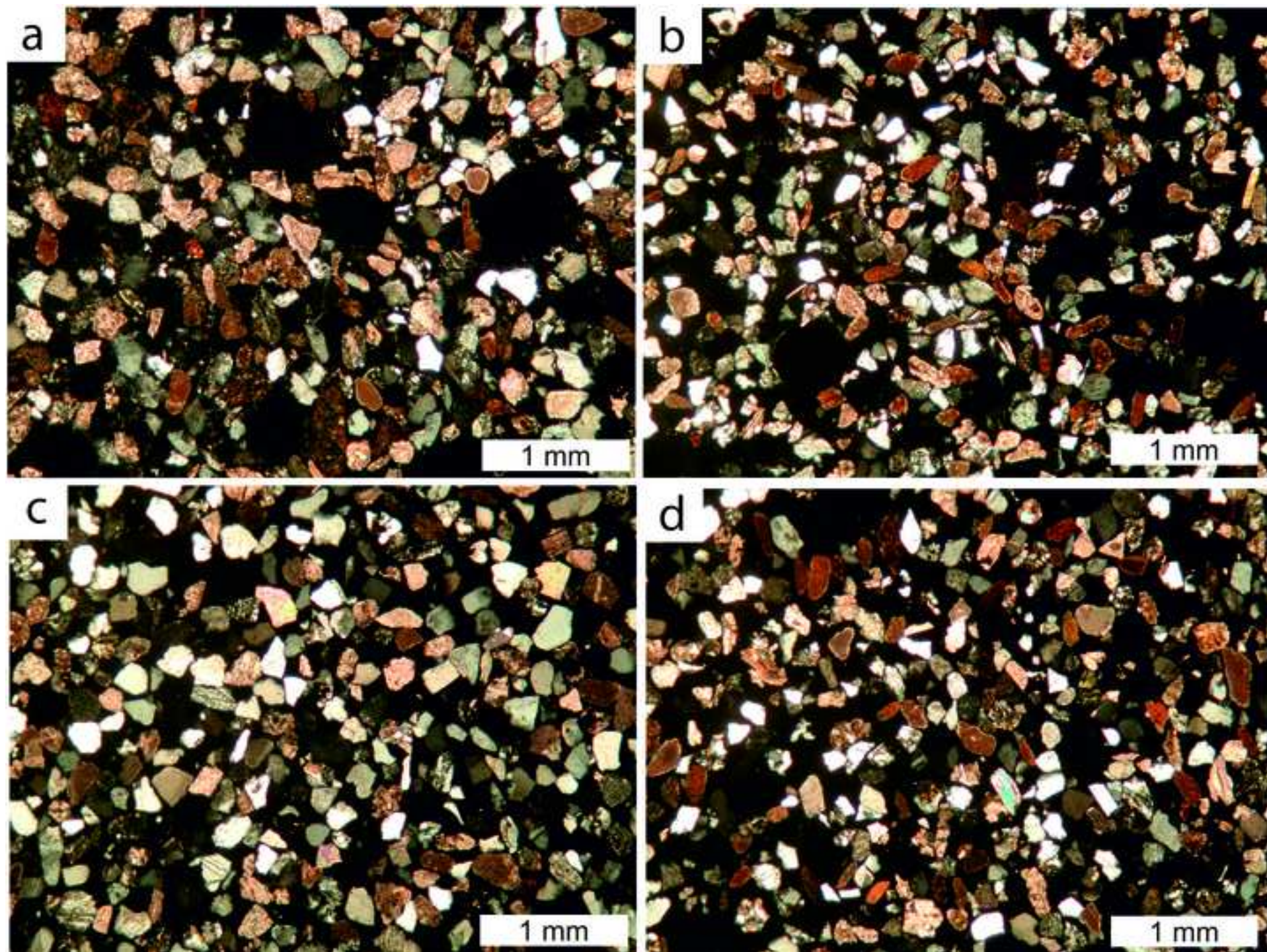


Figure 11

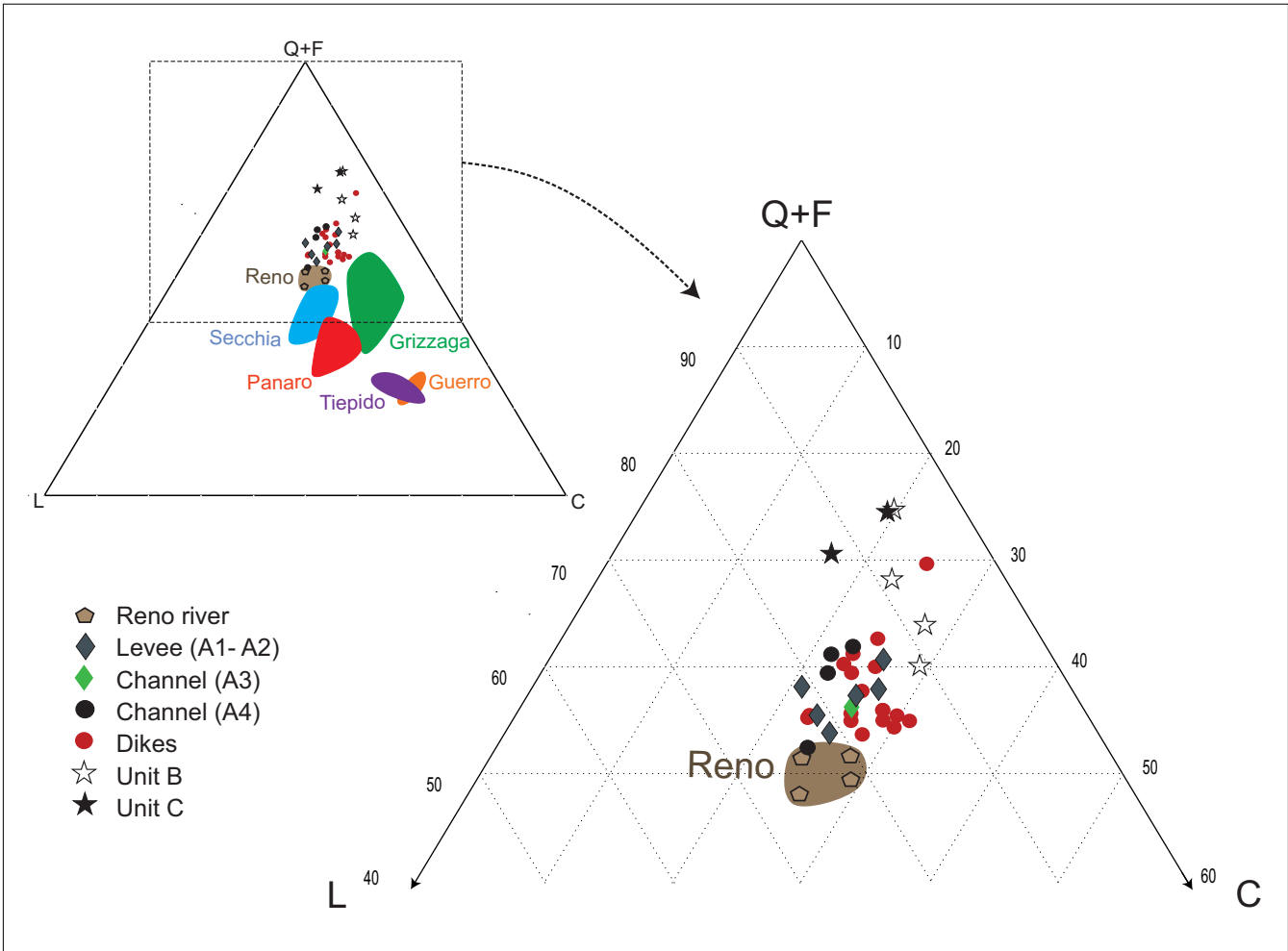


Figure 12

